Research Article

Gulfem Susoy*, Ghada ALMisned, Shams A. M. Issa, Hesham M. H. Zakaly, Duygu Sen Baykal, Gokhan Kilic, Hessa Alkarrani, Antoaneta Ene, and Huseyin Ozan Tekin

PbO-doped K_2O–BaO–Al_2O_3–B_2O_3–TeO_2-glasses: Mechanical and shielding efficacy

https://doi.org/10.1515/phys-2025-0233
received February 25, 2025; accepted October 11, 2025

Abstract: This study investigates the mechanical properties as well as the gamma-ray, neutron, alpha, and proton shielding capabilities of PbO-doped titanium-barium-borate based (TiO_2–BaO–B_2O_3–Al_2O_3–K_2O) glass-ceramic system. Using the Phy-X/PSD program, several gamma-ray shielding parameters such as linear attenuation coefficient (μ), mass attenuation coefficient (μ/ρ), half value layer (HVL), mean free path, effective atomic number (Z_{eff}), exposure buildup factor (EBF) and energy absorption buildup factor (EABF) were theoretically computed in the photon energy range of 0.015–15 MeV. Gamma-ray transmission factors (TFs) were evaluated using Particle and Heavy Ion Transport Code System. Additionally, the projected range (PR) values for protons and alpha in the study were computed using the Stopping and Range of Ions in Matter code. In addition to examining gamma, neutron, alpha, and proton shielding capabilities, the study also assessed elastic modulus, density, and average molecular weight. The mechanical properties for each glass sample were calculated using Makishima–Mackenzie model. The results show an inverse relationship between elasticity and PbO content, indicating a trade-off between mechanical rigidity and radiation shielding effectiveness. A higher PbO concentration (4.5%) significantly raises the molecular weight, density (2.80–3.55 g/cm^3), and effective atomic number, which leads to better attenuation. Sample G1, for instance, has HVL = 3.269 cm at 0.662 MeV, while sample G5 exhibits better shielding at 2.538 cm. PbO presence causes buildup factors (EBF/EABF) to rise, particularly at higher photon energies and penetration depths, which suggests increased absorption of secondary photons. Denser, lead-rich glasses are known to promote gamma attenuation, as seen by the continuous reduction in TF with increasing PbO content, thickness (0.5–3.0 cm), and photon energy (0.662, 1.1732, 1.3325 MeV). Neutron shielding effectiveness, measured by the effective removal cross section (Σ_R), improved with higher PbO, with G5 (PbO [4.5%], Σ_R = 0.071 cm^{-1}) demonstrating the promising performance. The G5 sample has the lowest PR (Φ) values for alpha (Φ_p) and protons (Φ_A) particles, indicating improved stopping power. Finally, comparative benchmarking against literature-reported glass types confirmed the superior protection against gamma rays of the G5 sample. These results demonstrate how PbO-doped titanium-barium-borate based glass-ceramics may be used for sophisticated radiation protection applications by striking a balance between improved shielding and controllable mechanical characteristics.

Keywords: glass shield, lead oxide, heavy-charged particles, elastic modulus

*** Corresponding author: Gulfem Susoy,** Department of Physics, Faculty of Science, Istanbul University, 34134, Istanbul, Türkiye, e-mail: susoy@istanbul.edu.tr, glfmsusoy972@gmail.com
Ghada ALMisned: Department of Physics, College of Science, Princess Nourah Bint Abdulrahman University, P.O. Box 84428, Riyadh, 11671, Saudi Arabia
Shams A. M. Issa: 3Department of Physics, Faculty of Science, University of Tabuk, Tabuk, Saudi Arabia
Hesham M. H. Zakaly: Physics Department, Faculty of Science, Al-Azhar University, Assiut Branch, Egypt; Institute of Physics and Technology, Ural Federal University, Ekaterinburg, Russian Federation
Duygu Sen Baykal: Faculty of Engineering and Architecture, Mechatronics Engineering, Istanbul Nisantasi University, 34398, Istanbul, Turkey
Gokhan Kilic: Department of Physics, Faculty of Science, Eskisehir Osmangazi University, 26040, Eskisehir, Turkey
Hessa Alkarrani: Research Institute for Medical and Health Sciences, University of Sharjah, 27272, Sharjah, United Arab Emirates; Department of Medical Diagnostic Imaging, College of Health Sciences, University of Sharjah, 27272, Sharjah, United Arab Emirates
Antoaneta Ene: Department of Chemistry, Physics and Environment, INPOLDE Research Center, Faculty of Sciences and Environment, Dunarea de Jos University of Galati, 47 Domneasca Street, 800008, Galati, Romania
Huseyin Ozan Tekin: Department of Medical Diagnostic Imaging, College of Health Sciences, University of Sharjah, 27272, Sharjah, United Arab Emirates; Computer Engineering Department, Faculty of Engineering and Natural Sciences, Istinye University, Istanbul 34396, Turkey

1 Introduction

In the area of radiation protection, the choice of materials plays a pivotal role in ensuring safety and efficacy. Glass has become a very promising option among the different

materials used for shielding because of its special set of qualities [1–5]. High transparency, ease of production, and the flexibility to customize their properties with a variety of modifying agents are key advantages of glass shields [6]. The versatility of glass, coupled with its ability to form stable [7], homogeneous structures [8], makes it an ideal choice for various radiation shielding applications, particularly in environments where both protection and visibility are paramount, such as medical imaging facilities, nuclear power plants, and research laboratories. To enhance the protective capabilities of glass shields, specific oxides are incorporated into the glass matrix [9–11].

Each component contributes distinct properties that collectively enhance the overall performance of the glass shield. It is of great importance to know the properties of these components. As a network modifier, potassium oxide (K_2O) reduces the glass' melting point and viscosity while improving its workability. These features make it easier to manufacture and process high-performance shielding glasses, even while specific radiation-shielding data are few [12]. In order to maintain structural integrity, glass' amorphous network is usually constructed around a network former. Depending on composition, lead oxide (PbO) can behave as an intermediate oxide in certain systems, but it often acts as a network modifier. In order to create non-bridging oxygens (NBOs), Pb^{2+} ions interact with oxygen atoms at the atomic level, breaking the network and decreasing connection. In addition to increasing amorphousness and changing characteristics like density, these NBOs also reduce structural order. By forming areas of high electron density, Pb^{2+} also improves photon interactions because of its wide ionic radius and high atomic number. Hence, PbO enhances the glass' total density and refractive index, greatly enhancing its capacity to attenuate gamma rays. Superior shielding capability is indicated by Pb-doped glasses' lower half-value layers (HVLs), increased mass, and linear attenuation coefficients (LAC). PbO also improves clarity and brilliance, which is helpful in applications that call for vision through the shield [13]. Barium oxide (BaO) increases glass durability and refractive index [14]. Additionally, it facilitates easier production by lowering viscosity and melting temperature. Adding BaO also improves shielding performance, especially when combined with other modifiers like PbO [13]. Aluminum oxide (Al_2O_3) strengthens the glass structure by increasing hardness, chemical resistance, and thermal stability especially in the presence of strong radiation doses or harsh environmental conditions [15]. By acting as a glass forming, boron trioxide (B_2O_3) improves resilience to thermal shock and decreases thermal expansion. Additionally, it facilitates more uniform component mixing during melting. However, as seen in tellurite-glass investigations where heavier oxides provide higher gamma attenuation, adding too much B_2O_3 can reduce density and shielding capabilities [16,17]. Titanium dioxide (TiO_2) increases the refractive index and UV absorption of glass [18]. It also enhances chemical durability and mechanical strength, contributing to the longevity and effectiveness of the glass shield in harsh radiation environments.

The development of glass-ceramics with enhanced radiation shielding properties has been extensively studied. For example, it has been demonstrated that adding heavy metal oxides (HMO), such as PbO and BaO, to the glass matrix greatly increases the gamma-ray attenuation coefficients [19,20]. Lead oxide glasses are particularly noted for their high density and excellent radiation shielding capabilities [21]. Barium titanate-based glasses have also gained attention for their dielectric properties and ability to form stable crystalline phases, which are beneficial for radiation shielding and other electronic applications [22,23]. The addition of Al_2O_3 has been demonstrated to enhance the mechanical and thermal stability of glass-ceramics, making them more resistant to radiation damage [24]. Boron oxide, a well-known network former in glass chemistry, significantly improves the thermal and chemical stability of glasses [25]. Its incorporation has been shown to reduce the thermal expansion coefficient and enhance resistance to thermal shock, which is critical for maintaining the integrity of the glass shield in fluctuating temperatures [26]. Titanium dioxide, with its high refractive index and UV absorption properties, has been extensively used in the development of photocatalytic materials [27]. In glass-ceramics, TiO_2 enhances mechanical strength and chemical durability, contributing to the overall robustness of the shielding material [28]. The inclusion of K_2O and B_2O_3 enhances the workability and thermal stability of the glass, making it more resistant to thermal shocks and easier to fabricate into complex shapes. Barium oxide further contributes to the refractive index and chemical durability, ensuring that the glass remains clear and durable even under prolonged radiation exposure. The synergy of these components can produce a glass with optimized properties, balancing density, durability, and ease of fabrication, making it appropriate for a variety of radiation shielding applications [29–33].

This study investigates the mechanical properties as well as the gamma-ray, neutron, alpha, and proton shielding capabilities of PbO-doped titanium-barium-borate based TiO_2–BaO–B_2O_3–Al_2O_3–K_2O glass-ceramic system. Given the lack of studies on the addition of high-density PbO to titanium-barium-borate based glass-ceramic and the distinctive properties of the compounds in this glass-ceramic system, combining these compounds (K_2O, PbO, BaO, Al_2O_3, B_2O_3,

and TiO_2) [34] into a single glass system offers the potential to create a material with superior shielding properties. Also, the addition of HMOs, such as PbO and BaO, to the glass sample significantly increases the gamma-ray attenuation coefficients, which distinguishes this study from other studies. By hypothetically examining the gamma-ray, neutron, alpha, and proton shielding characteristics as well as the elastic modulus of these glasses, this study aims to address this gap. By understanding the synergistic effects of these components, one can design and develop a new class of glass-ceramics with enhanced radiation shielding properties. The findings of this study would open the door for the use of glass-ceramics with tailored properties, paving the way for their application in nuclear medicine, power plants, and other critical areas requiring advanced radiation protection solutions.

2 Materials and methods

As illustrated in Figure 1, schematic representation of the methodological workflow used for mechanical and radiation shielding analysis of PbO-doped titanium-barium-borate-based glass-ceramic samples was employed. The process begins with determining the glass inputs and calculating the average molecular weights necessary for subsequent analyses. This step is crucial for establishing the foundational properties of glass compositions. Following this, the glass samples' mechanical characteristics, such as the elastic modulus, are evaluated to assess their structural integrity and suitability for various applications. Concurrently, the gamma-ray, neutron, alpha, and proton shielding properties of the glass samples are analyzed to understand their effectiveness in radiation shielding. The results from these analyses are then benchmarked against existing data to validate and compare the performance of the glass samples.

2.1 Elastic modulus calculations

The glass samples, labeled G1 through G5, with specific molar compositions comprising TiO_2, K_2O, BaO, PbO, Al_2O_3, and B_2O_3 were investigated in terms of elastic modulus calculations. The Makishima-Mackenzie (MM) model is a theoretical approach widely applied in materials science to link the elastic properties of glassy systems with their chemical composition and structural parameters [35,36]. Based on the

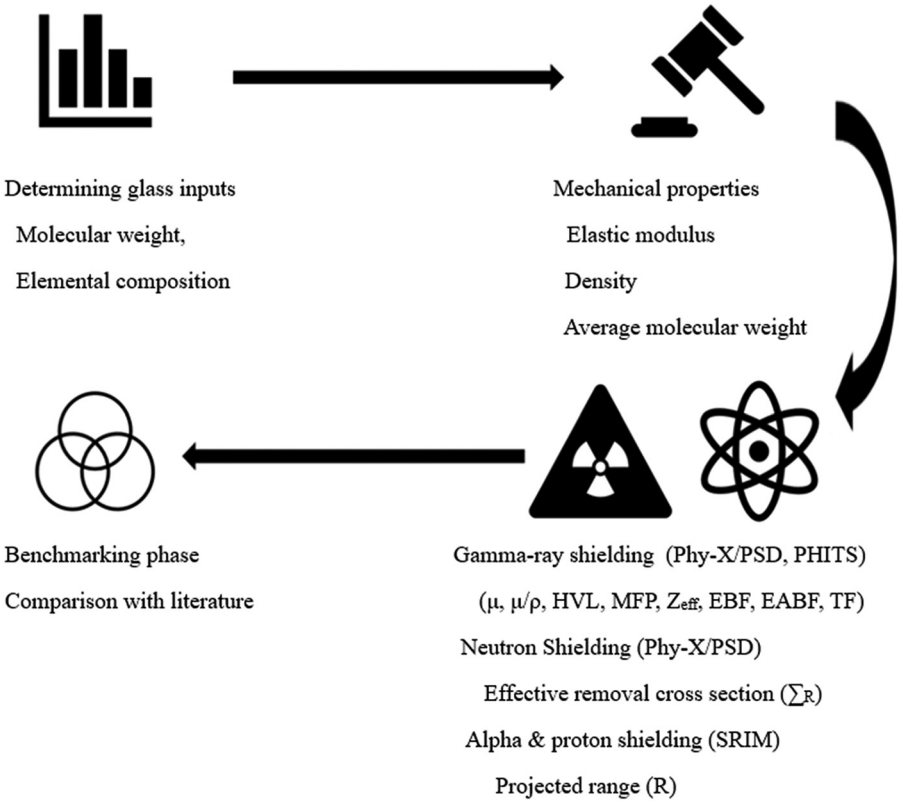

Figure 1: Schematical representation of the characterization process.

compositional analysis of the investigated glasses, two essential parameters packing density (V_t) and dissociation energy per unit volume (G_t) were calculated. These values were subsequently used to derive the main mechanical constants, including shear modulus (G), longitudinal modulus (L), Young's modulus (Y), bulk modulus (K), and Poisson's ratio (σ). This predictive framework enabled a comprehensive evaluation of the mechanical performance of the glass samples without relying solely on experimental testing, thereby providing valuable insight into the relationship between structure and mechanical behavior.

$$V_t = \frac{1}{V_m}\sum_i x_i V_i, \tag{1}$$

$$V_i = N_A\left(\frac{4\pi}{3}\right)(xR_A^3 + yR_O^3), \tag{2}$$

$$Y = 9.38 V_t G_t(\text{GPa}), \tag{3}$$

$$K = 10 V_t^2 G_t(\text{GPa}), \tag{4}$$

$$G = \frac{30 V_t^2 G_t}{(10.2 V_t - 1)}(\text{GPa}), \tag{5}$$

$$L = K + \left(\frac{4G}{3}\right)(\text{GPa}), \tag{6}$$

$$\sigma = \frac{Y}{2G} - 1. \tag{7}$$

Here R_A and R_O are the ionic radius of metal and oxygen, respectively. The mechanical parameters are obtained for PbO-doped titanium-barium-borate-based glass-ceramic samples using the equations given above.

2.2 Gamma-ray shielding parameters

Several gamma-ray shielding parameters were theoretically computed in order to assess the glass samples' gamma-ray shielding efficacy. These parameters include the LAC (μ), mass attenuation coefficient (MAC) (μ/ρ), mean free path (MFP), HVL, and buildup factors (exposure buildup factor [EBF] and energy absorption buildup factor [EABF] [7–10]. The calculations were theoretically computed in the photon energy range of 0.015–15 MeV using the Phy-X/PSD [37] software, a robust tool designed for radiation shielding analysis.

2.3 Neutron shielding parameters

Along with gamma-ray shielding parameters, the effectiveness of the synthesized glass samples in attenuating fast neutrons was evaluated. Fast neutrons, with energies typically above 1 MeV, interact with materials primarily through elastic and inelastic scattering, as well as neutron capture reactions. These interactions result in the reduction in neutron energy and eventual removal of neutrons from the beam. The probability that a neutron will be extracted from the incident neutron beam per unit route length is represented by the effective removal cross-section (Σ_R) [38]. It is measured in units of cm^{-1} and indicates how well a material attenuates fast neutrons. A material's ability to attenuate fast neutrons increases with its Σ_R value. The following formula can be used to potentially calculate the Σ_R values.

$$\sum_R = \sum_i (N_i \cdot \sigma_{R,i}). \tag{8}$$

The material's ith element's number density (in atoms/cm^3) is N_i, and its fast neutrons' microscopic removal cross-section is denoted by $\sigma_{R,i}$. The microscopic removal cross-section data ($\sigma_{R,i}$) used in this study were obtained using the Phy-X/PSD software, which is based on NIST-supported cross-section databases and established physical interaction models [37]. Using their number densities and microscopic cross-sections, the contributions from each element were added up to determine the (Σ_R) values for each glass sample.

2.4 Heavy-charged particles shielding parameters

A charged particle's total route length before coming to rest inside a substance is known as its projected range (PR) (R). It is a crucial factor in figuring out how thick the material needs to be to stop the particles entirely. PR of the radiation through the glass samples were evaluated using the Stopping and Range of Ions in Matter (SRIM) codes, developed by Ziegler *et al.* [39], which is one of the most widely used techniques for such calculations. The PR is computed by integrating the inverse of the stopping power over the particle's energy and is commonly given in units of g/cm^2 or cm.

$$R = \int_{E_0}^{0} \frac{1}{S(E)} dE, \tag{9}$$

where, R is the PR, E_0 is the initial energy of the particle, and $S(E)$ is the stopping power as a function of energy E.

2.5 Particle and Heavy Ion Transport Code System (PHITS) simulations for transmission factor (TF) values

The simulation incorporates physical processes like scattering and absorption to simulate how radiation interacts

with the alloy. T-track tallies, which measure photon flux and make it easier to calculate TFs for each alloy, are used to analyze the detector data. A monoenergetic gamma-ray source was used to measure the intensity of primary and secondary photons for the TF calculations. In order to accurately assess the material's shielding effectiveness, the TF was calculated as the ratio of photon intensity after passing through the alloy sample (I) to the original photon intensity (I_0). The simulated results closely match theoretical expectations and actual findings because of PHITS's shown dependability in modeling radiation interactions and attenuation processes. The TF values of the PbO-doped titanium-barium-borate-based TiO_2–BaO–B_2O_3–Al_2O_3–K_2O glass-ceramic system were evaluated in this study using PHITS simulations [40–43]. Figure 2 shows the simulation setup, which includes 2D and 3D models of the glass samples that are modeled and placed inside a lead block that contains a gamma-ray source. Photons with an energy of 1 MeV were to be emitted by the gamma-ray source. The material definition in the input file was modified to represent the unique elemental composition of each glass sample in order to guarantee an accurate simulation of the various glass compositions. A tally mesh was integrated inside the cell with the glass cover for detection and measuring purposes. A significant number of particle histories (NPS 10^8) were used in each simulation to guarantee statistical reliability. The overall relative error from the simulations is less than 0.1%, demonstrating the accuracy of our results. A high-performance LENOVO® P640 workstation, selected for its capacity to manage the complex numerical computations needed by the PHITS code, was used to carry out the computational operations.

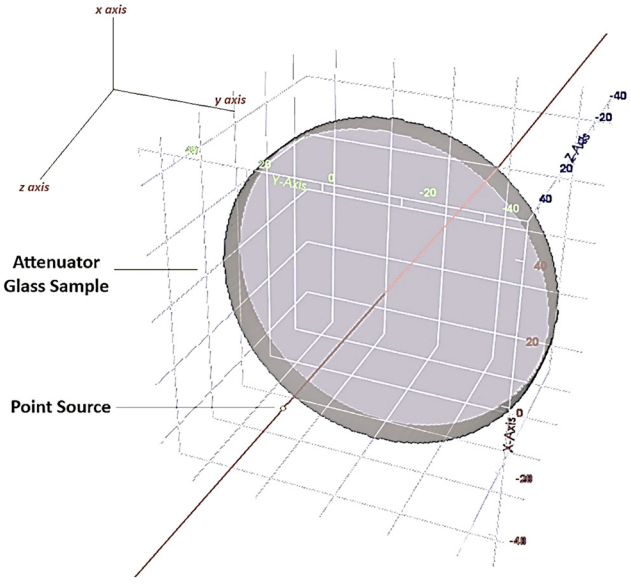

Figure 2: 2D and 3D views of modeled setup for TF calculations in PHITS.

3 Results and discussion

3.1 Elastic modulus properties of the glasses

The analysis of the calculated values reveals distinct variations in the mechanical performance of the investigated glass samples. The results obtained for each glass sample are given in Table 1. The molar volume is highest in G1 (36.19 cm^3/mol) and gradually decreases toward G5 (29.33 cm^3/mol). In contrast, V_t increases from 0.45 in G1 to 0.56 in G5, indicating the formation of a more compact structure with more efficiently packed atoms. G_t values are generally around 19 GPa, with G2 showing the lowest value (16.84 GPa), suggesting weaker bond strength compared to the other samples. Y increases from 73.88 GPa in G1 to above 90 GPa in G4 and G5, clearly reflecting the correlation between higher V_t and enhanced rigidity of the glasses. Both K and G follow an increasing trend from G1 to G5. While K rises from 40.14 GPa in G1 to 60.27 GPa in G5, G increases from 33.14 to 38.49 GPa. These results imply that the glasses become less compressible and more resistant to shear deformation as the composition evolves. Similarly, L varies between 82.24 GPa (G2) and 112.11 GPa (G4), with a marked improvement observed in G3–G5, consistent with the increase in density and bonding strength. σ ranges from 0.19 in G1 to 0.25 in G4–G5. Lower values indicate a more brittle nature, whereas higher values close to 0.25 suggest a shift toward a tougher, more ductile behavior. Overall, the findings highlight that G4 and G5 exhibit superior elastic moduli and relatively higher σ values, making them the mechanically strongest glass compositions within the investigated series.

3.2 Average molecular weight and density variations

Figure 3 shows that the density and average molecular weight of glass samples (G1–G5) both dramatically increase when the PbO level rises. The exact compositions of samples G1 through G5, where the proportions of other components stay constant but the PbO level varies, are shown in Table 2. It is clear that there is an increased trend in the density of the glass samples as the PbO content rises. From G1 to G5, the manufactured sample's ρ rises from 2.80 to 3.55 g/cm^3. The rising PbO

Table 1: Mechanical parameters of the investigated PbO-doped titanium-barium-borate-based (TiO_2–BaO–B_2O_3–Al_2O_3–K_2O) glass-ceramic system

Sample	M (g/mol)	Molar volume (cm^3/mol)	V_t	G_t	Young's Y (Gpa)	Bulk K (Gpa)	Shear G (Gpa)	Longitudinal L (Gpa)	Poisson's σ
G1	101.34	36.19	0.45	19.45	73.88	40.14	33.14	84.34	0.19
G2	102.04	33.13	0.50	16.84	69.83	41.42	30.62	82.24	0.22
G3	102.74	31.32	0.52	19.39	84.92	53.23	36.75	102.24	0.23
G4	103.44	29.30	0.56	19.35	90.54	60.61	38.62	112.11	0.25
G5	104.13	29.33	0.56	19.32	90.21	60.27	38.49	111.59	0.25

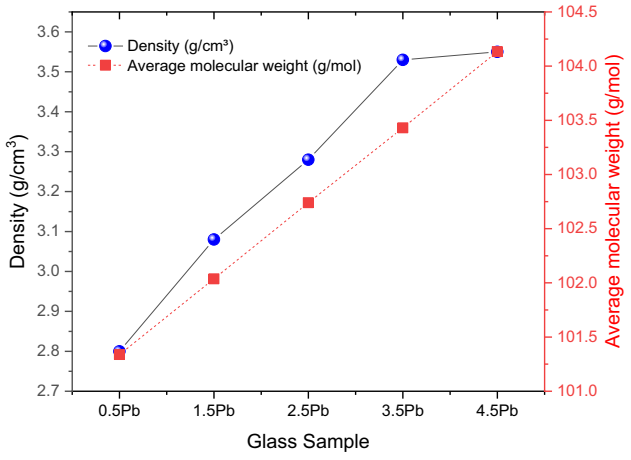

Figure 3: Variation in glass densities and average molecular weights as a function of PbO contribution.

concentration is the cause of this trend. This finding is consistent with the fact that Pb has a substantially larger atomic mass than the other elements (Ti, K, Ba, Al, B, and O) in the glass matrix. Density increases as a result of raising the PbO fraction since it increases the overall mass per unit volume. Likewise, as the PbO level rises, so does the average molecular weight of the glass samples. Once more, the addition of heavier Pb atoms to the glass network is the cause of this rise. Notable is the close relationship between density and average molecular weight, which both rise with more PbO. This link makes sense because density and molecular weight naturally increase as the glass structure gets denser and contains heavier atoms. This pattern is consistent with research from a variety of glass systems in literature. For example, studies on Lead-Borate (PbO–B_2O_3) glasses [44,45] have shown that density rises when PbO content increases, and molar volume, which is inversely related to molecular compactness, likewise rises, This confirms our finding that as mass per unit volume rises, heavier PbO additions produce denser glasses. Other studies on different glass systems also report a similar inverse relationship between density and molar volume, reinforcing the correlation with molecular compactness. For instance aluminum lead phosphate glass systems [46], TeO_2–CdO–PbO–B_2O_3 glass system [47], and lead-bismuth tellurite glass systems (TeO_2–Bi_2O_3–PbO) are some of them.

3.3 Properties of gamma-ray shielding

3.3.1 LAC

For the glass samples with compositions listed in Table 2, Figure 4 shows how the LAC change with incident photon energy and PbO contribution. The LAC values are observed to vary significantly with both the photon energy and the PbO content. At lower photon energies (<0.5 MeV), the photoelectric effect is the main process, the LAC values are substantially higher, indicating that the glass samples are highly effective in attenuating low-energy gamma photons. This is consistent across all PbO contributions, although higher PbO contents show more pronounced attenuation. This shows that all glass samples effectively attenuate low-energy photons. This tendency is anticipated as photoelectric absorption, which is heavily reliant on atomic number (Z), predominates at low energies. As the photon energy increases (0.5–1 MeV), the predominant interaction mechanism shifts to Compton scattering,

Table 2: Molar fractions (%) and densities (g/cm^3) of PbO-doped titanium-barium-borate-based [TiO_2–BaO–B_2O_3–Al_2O_3–K_2O] glass-ceramic system

Sample	TiO_2 (mol%)	K_2O (mol%)	BaO (mol%)	PbO (mol%)	Al_2O_3 (mol%)	B_2O_3 (mol%)	Density (g/cm^3)	Ref.
G1	38	9	23.5	0.5	16	13	2.80	[34]
G2	38	9	22.5	1.5	16	13	3.08	
G3	38	9	21.5	2.5	16	13	3.28	
G4	38	9	20.5	3.5	16	13	3.53	
G5	38	9	19.5	4.5	16	13	3.55	

the LAC values decrease sharply but the rate of decrease slows down. In the high energy region (>1 MeV), pair formation is the main process for γ-photons and attenuation exhibits a weak reliance on chemical composition. The reduced interaction probability for higher energy photons explains this tendency. However, samples with higher PbO content maintain higher LAC values compared to those with lower PbO content. The highest PbO content (4.5% PbO, G5) exhibits the highest LAC values, demonstrating superior gamma-ray attenuation properties. This improvement is explained by the fact that lead has a larger atomic number and density, which raises the likelihood of gamma photon interactions inside the glass matrix.

3.3.2 HVL and MFP

Table 2 details the molar fractions (%) and densities (g/cm^3) of the glasses under investigation. Figure 5 illustrates the variation in HVL, and Figure 6 presents the corresponding changes in MFP, both plotted as functions of input photon energy and PbO content. The HVL, which represents the thickness of material needed to cut gamma-ray intensity in half, offers vital information on how well the glass samples shield. The MFP, defined as the average distance travelled by a photon before undergoing an interaction such as absorption or scattering, serves as a crucial metric for assessing a material's shielding effectiveness. Specifically, a shorter MFP indicates more frequent photon interactions and thus superior radiation attenuation. It is evident from the data that photon energy and PbO content have a considerable impact on both HVL and MFP. HVL and MFP attain their lowest levels at low photon energies (below ~0.1 MeV), suggesting that all glass samples exhibit excellent attenuation of low-energy photons. Both parameters significantly increase with photon energy, indicating the decreased contact likelihood of higher-energy photons. Furthermore, there is a noticeable impact on the concentration of PbO: glasses with a higher PbO content consistently show improved attenuation performance,

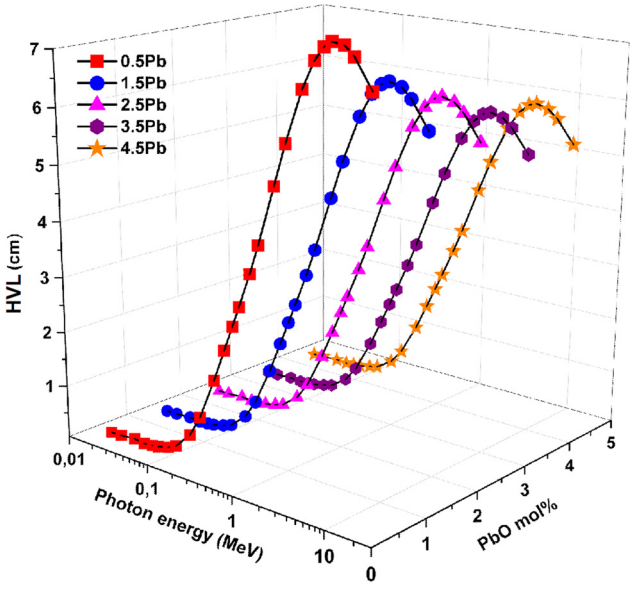

Figure 5: Variation in HVL as a function of incident photon energy and PbO contribution.

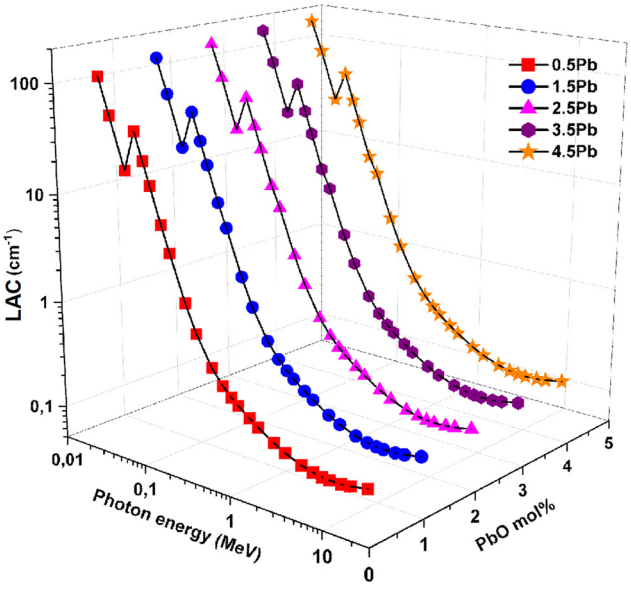

Figure 4: Variation in LAC as a function of incident photon energy and PbO contribution.

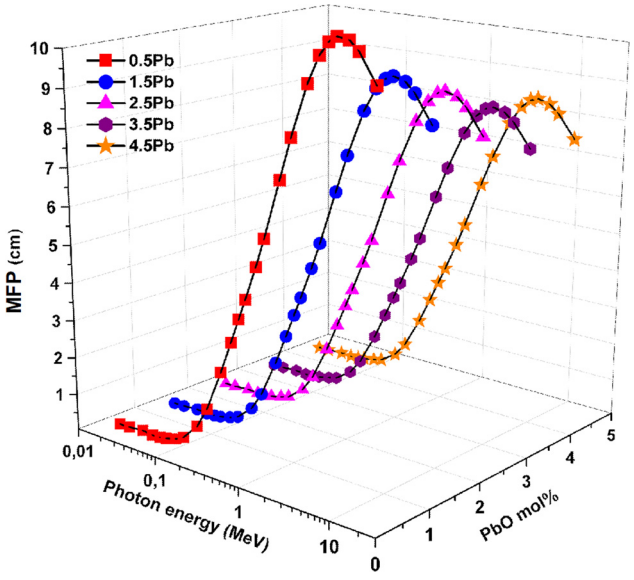

Figure 6: Variation in MFP as a function of incident photon energy and PbO contribution.

with lower HVL and MFP across all energy levels. The glass sample with 0.5% PbO (*i.e.*, G1) has the highest HVL and MFP values, implying the least effective shielding, while the sample with 4.5% PbO (G5) has the lowest HVL and MFP values, suggesting the best shielding efficacy. In this study, for the glass samples G1–G5, the HVL values at 1.173 MeV were found to decrease from 4.419 to 3.464 cm as the PbO content increased from 0.5 to 4.5 mol%. Similarly, in the $PbO–MoO_3–B_2O_3$ glass system reported in the literature [48], raising the PbO concentration from 30 to 50 mol% decreased the HVL from around 2.693 to 1.752 cm and the MFP from roughly 3.886 to 2.529 cm at the same photon energy. The high atomic mass and density of lead, which facilitate photon interactions and attenuation, are responsible for this enhancement. Consequently, adding more PbO greatly improves glass' ability to shield against gamma rays, particularly at higher photon energy.

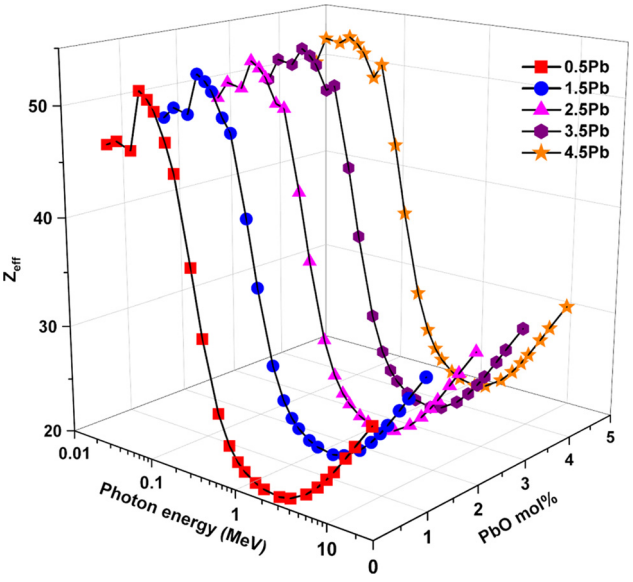

Figure 7: Variation in effective atomic number (Z_{eff}) values as a function of incident photon energy and PbO contribution.

3.3.3 Effective atomic number (Z_{eff})

The effective atomic number varies with photon energy and PbO concentration, as seen in Figure 7. Z_{eff} is heavily dependent on both variables, just like other shielding characteristics. Every sample shows high Z_{eff} values at photon energies <0.1 MeV, indicating strong photon interaction. As energy increases, Z_{eff} falls, reaches a minimum close to 1 MeV, and then slightly increases at higher energies. Because of the high atomic number of lead, glasses with a greater PbO content specifically, G5 (4.5% PbO) consistently exhibit higher Z_{eff} values than low-PbO samples, such as G1 (0.5% PbO). This confirms PbO's role in enhancing photon interaction probability and improving the glass' overall shielding effectiveness.

3.3.4 EBF and EABF

The EBF and EABF values for the glass samples range from 0.5 to 40 MFP, contingent on photon energy and PbO concentration, as shown in Figures 8(a–e) and 9(a–e). The EABF measures the amount of energy absorbed by the interacting material, whereas the EBF indicates the degree of contact between source and detector in the air. At low photon energies (0.01–0.1 MeV), EBF and EABF values are negligible, suggesting little secondary radiation accumulation. Both variables show a large rise with MFP in the intermediate range (0.1–1 MeV), particularly in the 4.5% PbO sample, indicating higher absorption and scattering. EBF and EABF continue to climb steadily at high energies (1–10 MeV), peaking close to 10 MeV. The 4.5% PbO sample once again exhibits the highest values at 40 MFP, demonstrating the significant influence of PbO concentration and penetration depth on radiation accumulation. Secondary radiation buildup is increased by higher PbO levels, particularly at higher MFP and intermediate to high photon energies. This pattern emphasizes how crucial it is to maximize PbO content in glass compositions in order to improve gamma-ray shielding.

3.4 Effective removal cross-section (Σ_R) values against fast neutrons

Figure 10 illustrates how the PbO content affects the Σ_R values. The attenuation of fast neutrons by the material is measured by Σ_R values. According to the findings, the PbO level of the glass samples causes an increase in Σ_R values. For instance, Σ_R values were reported as 0.5% PbO (G1): Σ_R = 0.060 cm^{-1}, 1.5% PbO (G2): Σ_R = 0.065 cm^{-1}, 2.5% PbO (G3): Σ_R = 0.068 cm^{-1}, 3.5% PbO (G4): Σ_R = 0.070 cm^{-1}, 4.5% PbO (G5): Σ_R = 0.071 cm^{-1}, respectively. Higher PbO content results in an increase in Σ_R, which suggests that PbO improves the glass' capacity to attenuate fast neutrons. The reason for this is that the high atomic mass and neutron cross-section of lead encourage neutron interactions inside the glass matrix. A higher PbO content considerably enhances neutron shielding, as evidenced by the steady increase in Σ_R values, which peaks in the 4.5% PbO sample. These findings highlight how crucial it is to optimize PbO levels for improved shielding effectiveness.

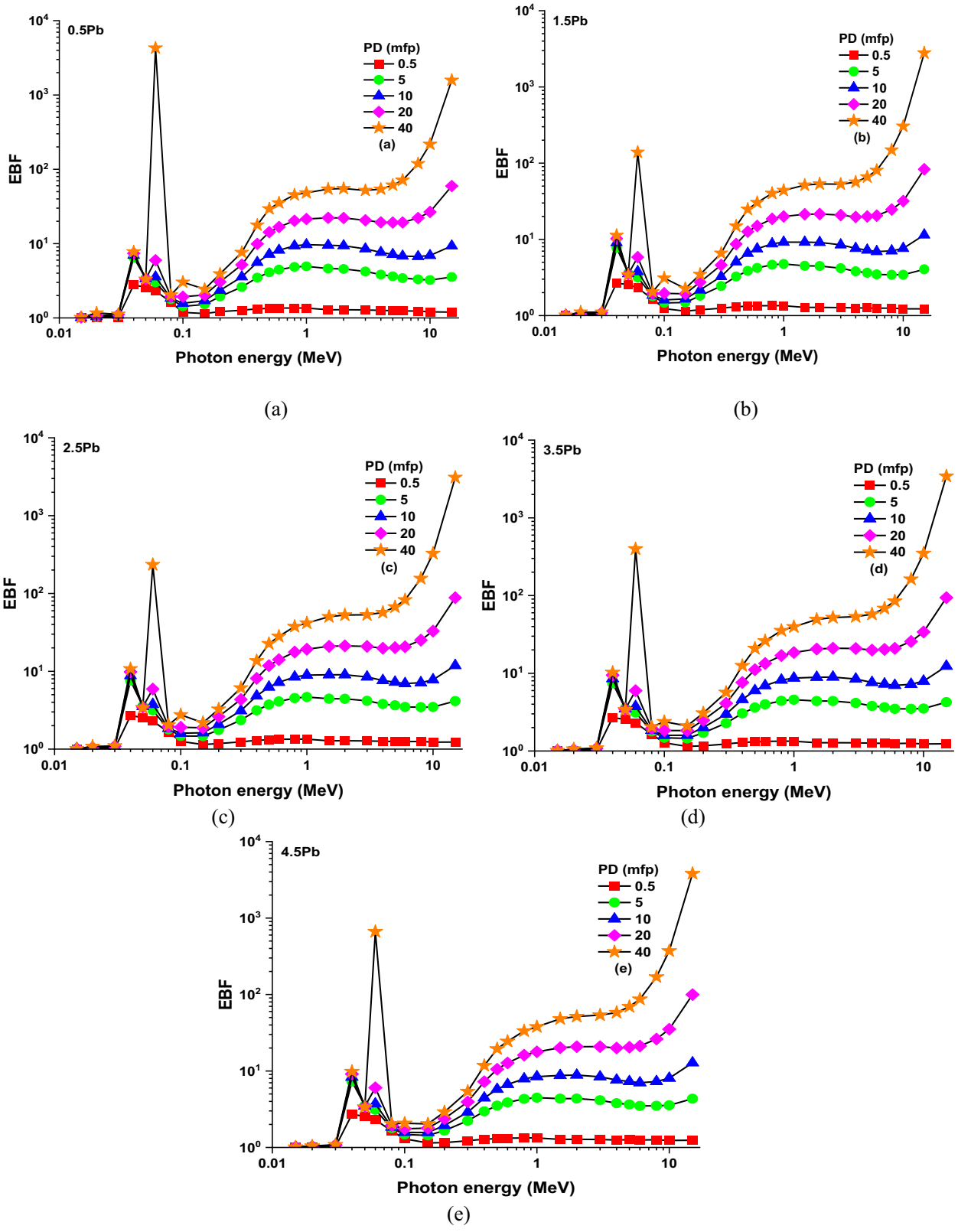

Figure 8: (a)–(e): Variation in EBF values as a function of incident photon energy and PbO contribution at different MFPs (*i.e.*, from 0.5 to 40 MFP).

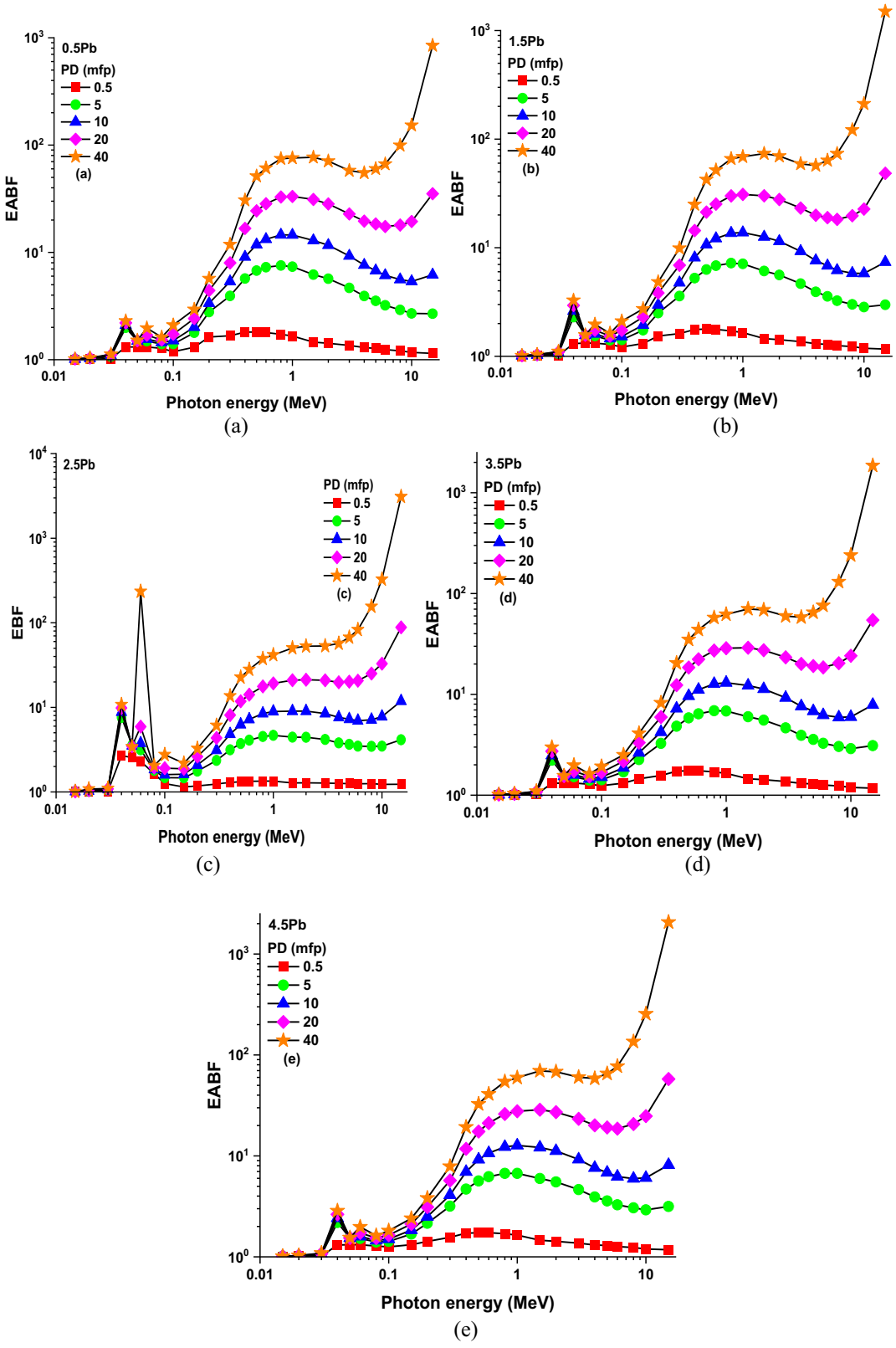

Figure 9: (a)–(e): Variation in EABF values as a function of incident photon energy and PbO contribution at different MFPs (*i.e.*, from 0.5 to 40 MFP).

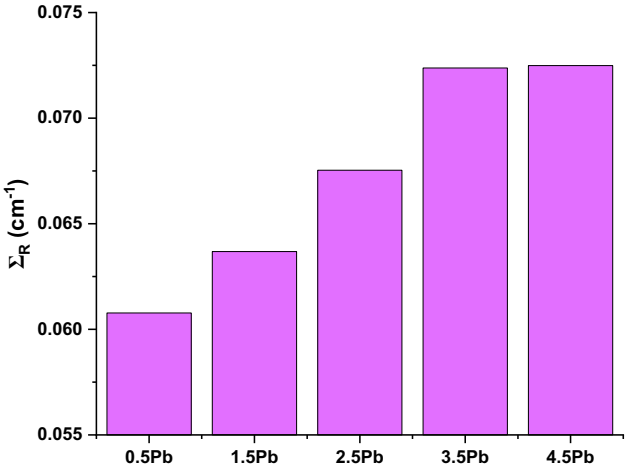

Figure 10: Variation in effective removal cross-section ($\sum_R$) values.

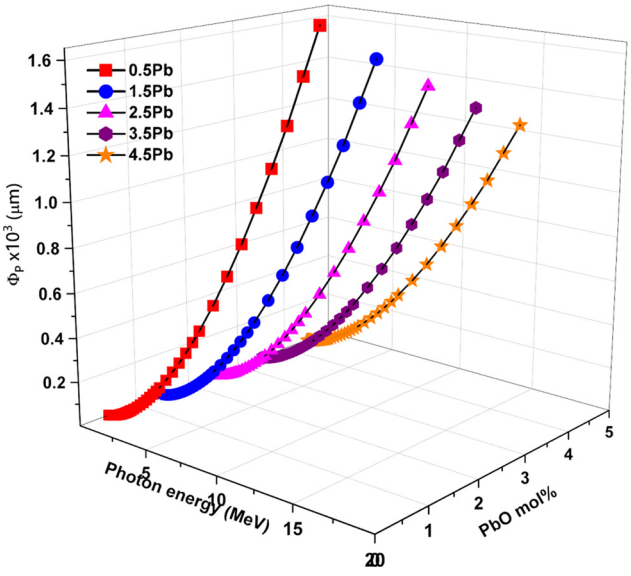

Figure 11: PR (Φ_P) values of the glasses against energetic protons.

3.5 PR values for proton and alpha particles

PR of the radiation through the glass samples were evaluated using the SRIM codes. Figures 11 and 12 present the PR (Φ) values of the glass samples against energetic protons (Φ_P) and alpha particles (Φ_A), respectively. These values indicate the depth at which the particles are expected to be stopped within the material, providing insight into the material's shielding effectiveness. In all glass samples, the PR of protons (Φ_P) increases as photon energy increases. Higher PbO-containing samples, on the other hand, consistently exhibit lower Φ_P values, indicating improved proton stopping power.

0.5% PbO (G1) shows the highest PR values, suggesting the least effective proton stopping power while the 4.5% PbO (G5) depicts the lowest PR, demonstrating superior proton stopping capability. Likewise, the PR (Φ_A) for alpha particles rises with photon energy across all glass samples, with higher PbO content resulting in lower Φ_A values. The fact that alpha particles and protons behave similarly emphasizes how more PbO improves attenuation and stopping power. The higher atomic number and density of lead are the main causes of the decreased PR. The 4.5% PbO (G5) sample has the highest PbO content and the lowest PR values for both particle types, as shown in Figures 11 and 12.

3.6 TF values against energetic photons

As seen in Figure 13, the TF values for samples G1, G2, G3, G4, and G5 were examined for a range of sample thicknesses from 0.5 to 3.0 cm at three different radioisotope photon energies: 0.662, 1.1732, and 1.3325 MeV. These results obtained using PHITS show a similar trend: As sample thickness and PbO content increase across all energy levels, TF values fall. As sample thickness and PbO content increase, TF values drop at all photon energies examined (0.662, 1.1732, and 1.3325 MeV). The 4.5% PbO sample exhibits the lowest TF values, indicating the most effective gamma-ray shielding, whereas the 0.5% PbO sample consistently displays the highest TF values, indicating the poorest attenuation. The high atomic number and density of lead, which improve gamma-ray interaction inside the glass matrix, are responsible for this tendency. Because higher-energy photons have a better ability to penetrate, TF values increase with increasing energy for a given

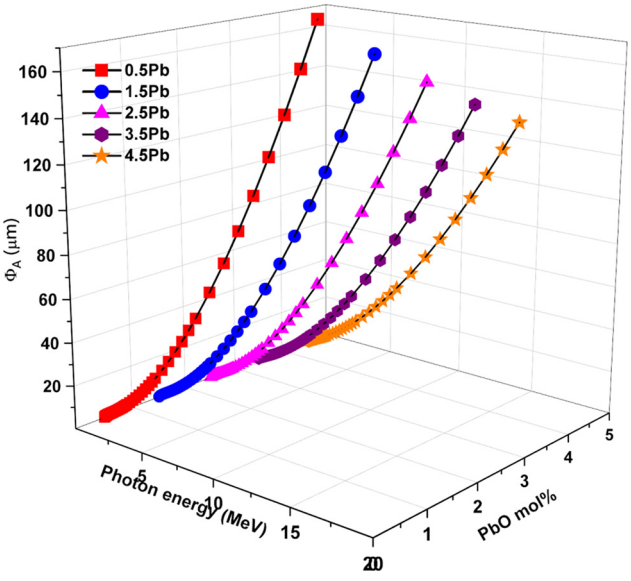

Figure 12: PR (Φ_A) values of the glasses against energetic alpha particles.

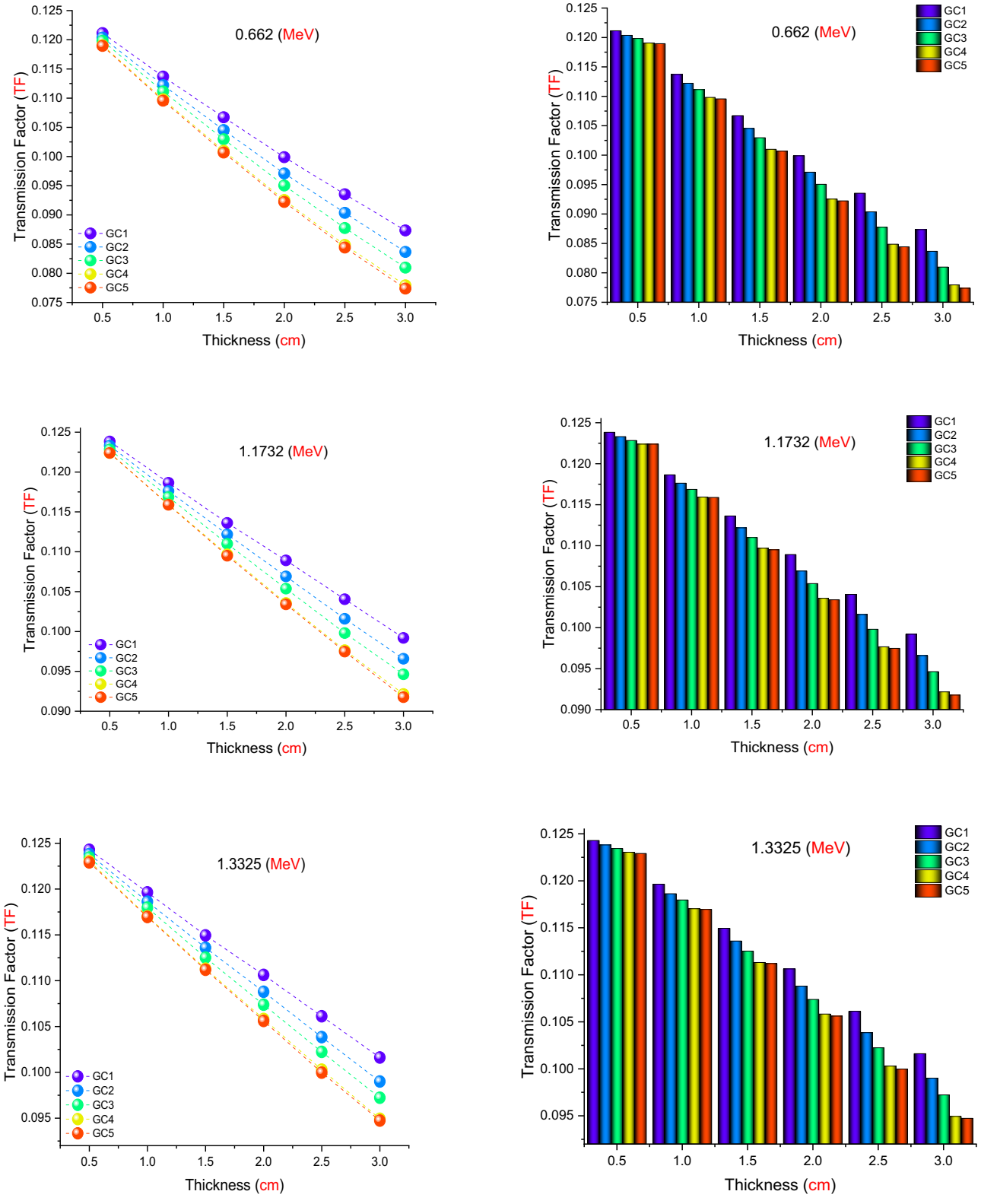

Figure 13: TFs for all investigated samples as a function of used radioisotope energy (MeV) at different sample thicknesses.

thickness. The highest TF values among the three energies are found at 1.3325 MeV, which is in line with the recognized difficulties of attenuating higher powerful gamma rays. Overall, for all thicknesses and energies, a definite inverse relationship between PbO concentration and TF values is seen. These findings demonstrate how crucial it is to maximize PbO content in glass formulations in order to guarantee effective gamma-ray shielding performance.

3.7 Benchmarking phase between the G5 (4.5% PbO) and other glasses

Table 3 and Figure 14 provide a comparative analysis of the HVL values for the glass samples G1–G5, alongside various glass compositions reported in the literature, including BCV0.5, BCBV0.5, S1, BSBaZn, and LBE5. Below 0.015 MeV, *i.e.*, at lower photon energies, the HVL values for the G1–G5 samples are notably low, with G1 at 0.010 cm, G2 at 0.009 cm, G3 at 0.008 cm, G4 at 0.007 cm, and G5 at 0.007 cm. In comparison, the HVL values for other glasses such as BCV0.5 (0.025 cm), S1 (0.008 cm), BSBaZn (0.006 cm), and LBE5 (0.028 cm) are significantly higher, indicating that the G1–G5 glasses are more effective at attenuating gamma rays at this energy level. The addition of PbO, which raises the atomic number and density improves the probability of gamma-ray interactions, is responsible for this better performance. The HVL values for every sample increase when the photon energy reaches 0.662 MeV, but the G1–G5 glasses continue to show better performance compared to the other glass types. For instance, at 0.662 MeV, G1 has an HVL of 3.269 cm, while G5 exhibits an HVL of 2.538 cm. In contrast, the HVL values for BCV0.5, BCBV0.5, S1, BSBaZn, and LBE5 are 3.026, 3.006, 2.746, 3.895, and 3.486 cm, respectively. The lower HVL

Table 3: Comparison of the HVL (cm) for different types of glass samples [34,43,48–53] as a function of photon energy

Energy (MeV)	G1 [34]	G2 [34]	G3 [34]	G4 [34]	G5 [34]	BCV0.5 [34]	BCBV0.5 [50]	S1 [51]	BSBaZn [52]	LBE5 [53]
0.015	0.010	0.009	0.008	0.007	0.007	0.025	0.025	0.008	0.006	0.028
0.02	0.021	0.019	0.017	0.015	0.014	0.056	0.057	0.013	0.013	0.040
0.03	0.064	0.056	0.050	0.044	0.042	0.169	0.173	0.037	0.040	0.111
0.04	0.041	0.038	0.036	0.034	0.035	0.341	0.347	0.078	0.061	0.220
0.05	0.073	0.067	0.064	0.060	0.061	0.540	0.549	0.137	0.110	0.361
0.06	0.116	0.107	0.102	0.096	0.097	0.736	0.744	0.212	0.178	0.477
0.08	0.237	0.218	0.207	0.195	0.197	1.056	1.060	0.398	0.363	0.792
0.1	0.385	0.334	0.299	0.266	0.254	1.281	1.281	0.237	0.598	0.519
0.15	0.857	0.749	0.677	0.607	0.582	1.621	1.614	0.547	1.237	1.035
0.2	1.312	1.158	1.057	0.955	0.925	1.839	1.829	0.894	1.775	1.498
0.2835	1.895	1.693	1.562	1.427	1.396	2.117	2.104	1.411	2.405	2.078
0.3	1.988	1.779	1.644	1.504	1.473	2.166	2.152	1.499	2.503	2.171
0.3471	2.223	1.996	1.851	1.699	1.670	2.297	2.282	1.727	2.752	2.407
0.4	2.449	2.204	2.050	1.887	1.858	2.435	2.419	1.949	2.992	2.635
0.5	2.803	2.531	2.362	2.180	2.154	2.675	2.657	2.297	3.376	2.999
0.6	3.102	2.807	2.623	2.426	2.401	2.896	2.877	2.587	3.707	3.311
0.6617	3.269	2.960	2.769	2.563	2.538	3.026	3.006	2.746	3.895	3.486
0.8	3.613	3.275	3.067	2.842	2.818	3.303	3.280	3.069	4.285	3.847
0.8261	3.674	3.331	3.120	2.891	2.867	3.353	3.330	3.126	4.355	3.912
1	4.061	3.685	3.453	3.203	3.178	3.676	3.651	3.481	4.800	4.320
1.173	4.419	4.011	3.761	3.489	3.464	3.981	3.953	3.805	5.213	4.699
1.333	4.723	4.288	4.022	3.732	3.707	4.249	4.220	4.080	5.566	5.028
1.5	5.018	4.557	4.274	3.967	3.940	4.515	4.484	4.341	5.908	5.349
2	5.776	5.245	4.920	4.566	4.535	5.237	5.202	5.012	6.778	6.215
2.506	6.400	5.811	5.450	5.057	5.023	5.884	5.844	5.571	7.477	6.988
3	6.899	6.263	5.873	5.449	5.411	6.436	6.394	6.019	8.026	7.649
4	7.668	6.959	6.523	6.050	6.005	7.389	7.342	6.726	8.831	8.796
5	8.197	7.437	6.968	6.461	6.411	8.159	8.109	7.227	9.350	9.729
6	8.562	7.765	7.274	6.742	6.688	8.780	8.728	7.583	9.677	10.491
8	8.971	8.131	7.613	7.053	6.992	9.702	9.649	8.007	9.980	11.639
10	9.132	8.274	7.743	7.170	7.106	10.321	10.268	8.200	10.038	12.423
15	9.101	8.239	7.705	7.129	7.060	11.153	11.104	8.256	9.821	13.492

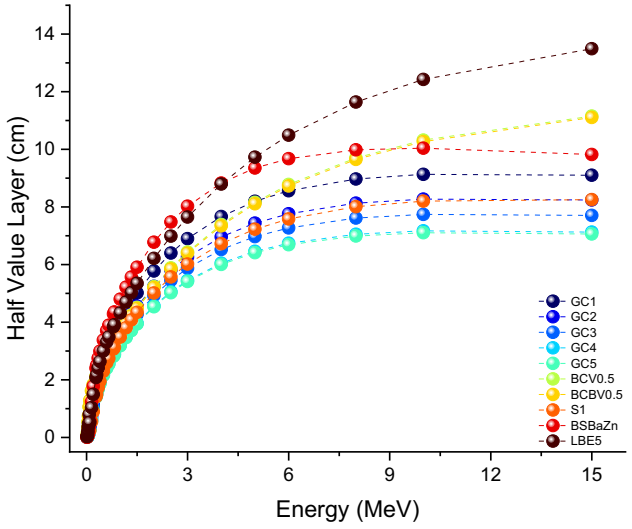

Figure 14: Comparison of HVL values.

values of G1–G5, particularly G5, indicate more effective attenuation, which is beneficial for radiation shielding applications. At higher photon energies, such as 1.3325 MeV, the trend continues. BSBaZn and BCV0.5 have HVL values of 4.320 and 3.847 cm, respectively, while G5 has an HVL of 3.464 cm. This demonstrates the superior gamma-ray attenuation capability of the G5 glass compared to other formulations. The HVL values for other glass samples from the literature, such as those studied by Ilik *et al.* [49,50], Barebita *et al.* [51], Sen Baykal *et al.* [52], and Chandrashekaraiah *et al.* [53], are generally higher across various photon energies. For example, Ilik *et al.* [49] investigated calcium-borate glasses (BCV0.5) doped copper(II) oxide and found them to have higher HVL values compared to our G5 sample. Similarly, Ilik *et al.* [50] studied calcium-borate glasses (BCBV0.5) doped vanadium(V) oxide and also reported higher HVL values. Barebita *et al.* [51] examined Bi_2O_3–P_2O_5–B_2O_3–V_2O_5 quaternary glass systems (S1) and found them to be less effective than our G5 sample at higher photon energies. Sen Baykal *et al.* [52] designed a lead-free high-density barium-borosilicate glass (BSBaZn), which also showed higher HVL values. Finally, Chandrashekaraiah *et al.* [53] studied $Li_2B_4O_7$ glasses doped with $Er3^+$ and Bi^{3+} ions (LBE5), which exhibited significantly higher HVL values across the energy spectrum.

4 Conclusion

This study investigates the mechanical properties as well as the gamma-ray, neutron, alpha, and proton shielding capabilities, elastic modulus, density, and average molecular weight of PbO-doped titanium-barium-borate-based [TiO_2–BaO–B_2O_3–Al_2O_3–K_2O] glass-ceramic system labeled G1–G5. Our findings reveal significant insights into the synergistic effects and inverse relationships between the components. The shielding parameters (LAC, HVL, MFP, Z_{eff}, Σ_R, EBF, EABF, and PR for proton and alpha particles were theoretically computed using the Phy-X/PSD program in the photon energy range of 0.015–15 MeV. Gamma-ray TF were evaluated using PHITS. Additionally, the PR values for protons and alpha in the study were computed using the SRIM code. The mechanical properties were evaluated using the MM model. An increase in the PbO ratio decreases the molar volume of the glass and increases the relative packing, resulting in a steady increase in Young's, bulk, shear, and longitudinal moduli. An increase in the Poisson ratio indicates that the glass structure becomes tighter, more rigid, and less flexible. With higher PbO levels, density and average molecular weight increase concurrently, improving radiation shielding due to increased atomic mass and compactness. Low photon energies had the highest LAC values, while higher photon energies resulted in lower values. Samples with higher PbO contents consistently displayed higher LAC values. G5 (4.5% PbO) demonstrated the best shielding performance, as evidenced by its lowest HVL. HVL values climbed with photon energy but fell with increasing PbO content. G5 continuously displayed lower HVL values than other glass compositions documented in the literature, demonstrating its remarkable gamma-ray shielding capability. According to sources [49–53], this benefit is particularly evident when contrasted with glasses like BCV0.5, BCBV0.5, S1, BSBaZn, and LBE5. Effective attenuation was demonstrated by MFP, which rose with energy but was lowest in high PbO samples. Z_{eff} rose in glasses with increased PbO, improving photon interaction, but it fell with energy. G5's remarkable neutron shielding capabilities was demonstrated by its greatest Σ_R value. The PRs (Φ) of protons and alpha particles decreased with increasing PbO content; G5 exhibited the shortest ranges, highlighting its effectiveness in stopping energetic particles. G5's exceptional performance was further validated by PHITS simulations, which consistently produced the lowest TF values across a range of gamma-ray energy and thicknesses, exhibiting exceptional attenuation.

At the atomic level, the network structure is changed when PbO is added to the glass matrix. It considerably raises the material's density and radiation-interaction capabilities while decreasing the structural regularity of the glass network. Although the mechanical strength may be slightly diminished as a result of this alteration, the radiation attenuation qualities are significantly improved. Applications in radiation shielding systems and nuclear technologies are especially sensitive to this impact.

It is possible to build and construct a unique class of glass-ceramics with higher radiation shielding qualities by comprehending the synergistic effects of these components. The results open the door for the use of these PbO-doped titanium-barium-borate-based glass-ceramics in nuclear medicine, power plants, and other vital industries that need cutting-edge radiation shielding technologies. These developments make the glass system a viable option for use in high-ionizing radiation settings, such as those found in the nuclear and medical industries, where remarkable shielding effectiveness and structural robustness are required. Its potential for incorporation into next-generation radiation protection systems is highlighted by this combination.

Acknowledgments: The authors would like to express their deepest gratitude to Assoc. Prof. Esra KAVAZ PERİŞANOĞLU for their valuable support and contributions to this work.

Funding information: The authors state no funding involved.

Author contributions: Gülfem SÜSOY DOĞAN: writing – review and editing, writing – original draft, visualization, methodology, investigation, formal analysis, and conceptualization. Ghada ALMisned: methodology, investigation, and formal analysis. Shams A.M. Issa: writing – original draft, validation, software, and investigation. Hesham M.H. Zakaly: material preparation, data collection, and analysis. Duygu Sen Baykal: material preparation, data collection, and analysis. Gokhan Kilic: methodology and investigation. Hessa Alkarrani: investigation, data curation, and writing – review. Antoaneta Ene: conceptualization, methodology, software, validation, and investigation. Huseyin Ozan Tekin: writing – original draft, visualization, methodology, investigation, formal analysis, and conceptualization. All authors have accepted responsibility for the entire content of this manuscript and approved its submission.

Conflict of interest: The authors state no conflict of interest.

Data availability statement: The datasets generated and/or analyzed during the current study are available from the corresponding author on reasonable request.

References

[1] Oto B, Yıldız N, Akdemir F, Kavaz E. Investigation of gamma radiation shielding properties of various ores. Prog Nucl Energy. 2015;85:391–403. doi: 10.1016/j.pnucene.2015.07.016.

[2] Singh VP, Badiger NM, Kaewkhao J. Radiation shielding competence of silicate and borate heavy metal oxide glasses: comparative study. J Non-Cryst Solids. 2014;404:167–73. doi: 10.1016/j.jnoncrysol.2014.08.003.

[3] Klein RC, Weilandics C. Potential health hazards from lead shielding. Am Ind Hyg Assoc J. 1996;57:1124–6. doi: 10.1080/15428119691014215.

[4] Ersundu Ç, Ersundu AE, Kityk IV. Investigation on gamma and neutron radiation shielding parameters for BaO/SrO–Bi_2O_3–B_2O_3 glasses. Radiat Phys Chem. 2018;145(4):26–33. doi: 10.1016/j.radphyschem.2017.12.010.

[5] Zanotto ED, Mauro JC. The glassy state of matter: its definition and ultimate fate. J Non-Cryst Solids. 2017;471:490–5. doi: 10.1016/j.jnoncrysol.2017.05.019.

[6] Mauro JC. Grand challenges in glass science. Front Mater. 2014;1(20):1–5. doi: 10.3389/fmats.2014.00020.

[7] Kurtulus R. Recent developments in radiation shielding glass studies: A mini-review on various glass types. Radiat Phys Chem. 2024;220:111701. doi: 10.1016/j.radphyschem.2024.111701.

[8] Karpuz N. Radiation shielding properties of glass composition. J Radiat Res Appl Sci. 2023;16(4):100689. doi: 10.1016/j.jrras.2023.100689.

[9] ALMisned G, Sen Baykal D, Susoy G, Kilic G, Zakaly MHH, Ene A, et al. Determination of gamma-ray transmission factors of WO_3–TeO_2–B_2O_3 glasses using MCPX Monte Carlo code for shielding and protection purposes. Appl Rheol. 2022;32(1):166–77. doi: 10.1515/arh-2022-0132.

[10] Sarihan M. Simulation of gamma-ray shielding properties for materials of medical interest. Open Chem. 2022;20(1):81–7. doi: 10.1515/chem-2021-0118.

[11] Boodaghi Malidarre R, Akkurt I. Evaluation of bioactive borosilicate added Ag glasses in terms of radiation shielding, structural, optical, and electrical properties. Silicon. 2022;14:12371–9. doi: 10.1007/s12633-022-01925-y.

[12] Fernandes HR, Tulyaganov DU, Goel A, Ribeiro MJ, Pascual MJ, Ferreira JMF. Effect of Al2O3 and K2O content on structure, properties and devitrification of glasses in the Li_2O–SiO_2 system. J Eur Ceram Soc. 2010;30(10):2017–30. doi: 10.1016/j.jeurceramsoc.2010.04.017.

[13] Sayyed MI, Hamad MK, Mhareb MHA, Naseer KA, Mahmoud KA, Khandaker MU, et al. Impact of Modifier Oxides on Mechanical and Radiation Shielding Properties of B_2O_3-SrO-TeO_2-RO Glasses (Where RO = TiO_2, ZnO, BaO, and PbO). Appl Sci. 2021;11(22):10904. doi: 10.3390/app112210904.

[14] Kaewjaeng S, Kaewkhao J, Limsuwan P, Maghanemi U. Effect of BaO on Optical, Physical and Radiation Shielding Properties of SiO_2-B_2O_3-Al_2O_3-CaO-Na_2O Glasses System. Procedia Eng. 2012;32:1080–6. doi: 10.1016/j.proeng.2012.02.058.

[15] Al-Ghamdi H, Sayyed I, Kumar A, Yasmin S, Elbashir BO, Almuqrin AH. Effect of PbO and B_2O_3 on the Physical, Structural, and Radiation Shielding Properties of PbO-TeO_2-MgO-Na_2O-B2O3 Glasses. Sustainability. 2022;14(15):9695. doi: 10.3390/su14159695.

[16] Yin S, Wang H, Wang S, Zhang J, Zhu Y. Effect of B_2O_3 on the Radiation Shielding Performance of Telluride Lead Glass System. Crystals. 2022;12(2):178. doi: 10.3390/cryst12020178.

[17] Abouhaswa AS, Abdelghany AM, Alfryyan N, Alsaif NAM, Rammah YS, Nabil IM. The impact of B_2O_3/Al_2O_3 substitution on physical properties and γ-ray shielding competence of aluminum-borate glasses: comparative study. J Mater Sci: Mater Electron. 2024;35:845. doi: 10.1007/s10854-024-12629-x.

[18] Singh GP, Singh J, Kaur P, Singh T, Kaur R, Kaur S, et al. Impact of TiO_2 on radiation shielding competencies and structural, physical and optical properties of CeO_2–PbO–B_2O_3 glasses. J Alloy Compd. 2021;885:160939. doi: 10.1016/j.jallcom.2021.160939.

[19] Takahashi J, Nakano H, Kageyama K. Fabrication and dielectric properties of barium titanate-based glass-ceramics for tunable microwave LTCC application. J Eur Ceram Soc. 2006;26(10–11):2123–7. doi: 10.1016/j.jeurceramsoc.2005.09.070.

[20] Ruiz-Valdez JJ, Gorokhovsky AV, Escalante-García JI, Mendoza-Suarez G. Glass-ceramics materials with regulated dielectric properties based in the system BaO-PbO-TiO_2-B_2O_3-Al_2O_3. J Eur Ceram Soc. 2004;24(6):1505–8. doi: 10.1016/S0955-2219(03)00531-4.

[21] Shi R, Pu Y, Wang W, Shi Y, Li J, Guo X, et al. Flash sintering of barium titanate. Ceram Int. 2019;45(5):7085–9. doi: 10.1016/j.ceramint.2018.12.211.

[22] González MA, Gorokhovsky A, Escalante JI, Ponce P, Escobedo MA. Crystallization and properties of glass-ceramics of the K_2O-BaO-B_2O_3-Al_2O_3-TiO_2 system. Mater Sci Forum. 2013;755:125–32. doi: 10.4028/www.scientific.net/MSF.755.125.

[23] Mandal RK, Prasad CD, Parkash O, Kumar D. Dielectric behaviour of glasses and glass ceramics in the system BaO-PbO-TiO_2-B_2O_3-SiO_2. Bull Mater Sci. 1987;9(4):255–62. doi: 10.1007/BF02743974.

[24] Huang YX, Senos AMR. Effect of the powder precursor characteristics in the reaction sintering of aluminium titanate. Mater Res Bull. 2002;37(1):99–111. doi: 10.1016/S0025-5408(01)00802-9.

[25] Barbieri L, Karamanov A, Corradi A, Lancellotti I, Pelino M, Rincon JM. Structure, chemical durability and crystallization behavior of incinerator-based glassy systems. J Non-Cryst Solids. 2008;354(6–7):521–8. doi: 10.1016/j.jnoncrysol.2007.07.080.

[26] Gautam C, Yadav AK, Singh AK. A review on infrared spectroscopy of borate glasses with effects of different additives. ISRN Ceram. 2012;2012:428497. doi: 10.5402/2012/428497.

[27] Escobedo Bretado MA, González Lozano MA, Collins Martínez V, López Ortiz A, Meléndez Zaragoza M, Lara RH, et al. Synthesis, characterization and photocatalytic evaluation of potassium hexatitanate ($K_2Ti_6O_{13}$) fibers. Int J Hydrogen Energy. 2019;44(24):12470–6. doi: 10.1016/j.ijhydene.2018.06.085.

[28] Savio AKPD, Fletcher J, Robles Hernández FC. Sonosynthesis of nanostructured TiO_2 doped with transition metals having variable bandgap. Ceram Int. 2013;39(3):2753–65. doi: 10.1016/j.ceramint.2012.09.042.

[29] Oruc Ulas E, Acikgoz A, Aktas B, Kavun Y. Influence of B_2O_3 incorporation on the structural, mechanical and radiation shielding properties of TeO_2 based bioglasses. Appl Radiat Isotopes. 2025;221:111799. doi: 10.1016/j.apradiso.2025.111799.

[30] Rasul SY, Aktas B, Yilmaz D, Pathman AF, Yalcin Ş, Acikgoz A. Impact of HfO2 on the structural, thermal, gamma, and neutron shielding properties of boro-tellurite glasses. Inorg Chem Commun. 2025;174(Part 1):113993. doi: 10.1016/j.inoche.2025.113993.

[31] Dogru K, Aktas B, Acikgoz A, Yilmaz D, Pathman AF, Yalcin Ş, et al. Structural, thermal, and radiation shielding properties of B2O3-TeO2-Bi2O3-CdO-Tm2O3 glasses: The role of Tm2O3. Ceram Int. 2024;50(22Part B):47384–94. doi: 10.1016/j.ceramint.2024.09.088.

[32] Solak BB, Aktas B, Yilmaz D, Kalecik S, Yalcin Ş, Acikgoz A, et al. Exploring the radiation shielding properties of B_2O_3-PbO-TeO_2-CeO_2-WO_3 glasses: A comprehensive study on structural, mechanical, gamma, and neutron attenuation characteristics. Mater Chem Phys. 2024;312:128672. doi: 10.1016/j.matchemphys.2023.128672.

[33] Aktas B, Yalcin S, Dogru K, Uzunoglu Z, Yilmaz D. Structural and radiation shielding properties of chromium oxide doped borosilicate glass. Radiat Phys Chem. 2019;156:144–9. doi: 10.1016/j.radphyschem.2018.11.012.

[34] Ponce-Peña P, González Lozano MA, Escobedo-Bretado MÁ, Núñez-Ramírez DM, Rodríguez-Pulido A, Quiñones Jurado ZV, et al. Crystallization of Glasses Containing K_2O, PbO, BaO, Al_2O_3, B_2O_3, and TiO_2. Crystals. 2022;12:574. doi: 10.3390/cryst12050574.

[35] Makishima A, Mackenzie JD. Direct calculation of Young's modulus of glass. J Non-Cryst Solids. 1973;12:35–45. doi: 10.1016/0022-3093(73)90053-7.

[36] Makishima A, Mackenzie JD. Calculation of bulk modulus, shear modulus and Poisson's ratio of glass. J Non-Cryst Solids. 1975;17:147–57. doi: 10.1016/0022-3093(75)90047-2.

[37] Şakar E, Özpolat ÖF, Alım B, Sayyed MI, Kurudirek M. Phy-X/PSD: Development of a user friendly online software for calculation of parameters relevant to radiation shielding and dosimetry. Radiat Phys Chem. 2020;166:108496. doi: 10.1016/j.radphyschem.2019.108496.

[38] El-Khayatt AM. Calculation of fast neutron removal cross-sections for some compounds and materials. Ann Nucl Energy. 2010;37(2):218–22. ISSN 0306-4549 doi: 10.1016/j.anucene.2009.10.022.

[39] Ziegler JF, Ziegler MD, Biersack JP. The stopping and range of ions in matter. New York, NY, USA: Pergamon Press; 1985ISBN 978-0-08-021607-2.

[40] Sato T, Iwamoto Y, Hashimoto S, Ogawa T, Furuta T, Abe S, et al. Features of particle and heavy ion transport code system (PHITS) version 3.02. J Nucl Sci Technol. 2018;55(6):684–90. doi: 10.1080/00223131.2017.1419890.

[41] Iwase H, Niita K, Nakamura T. Development of general purpose particle and heavy ion transport Monte Carlo code. J Nucl Sci Technol. 2002;39(11):1142–51. doi: 10.1080/18811248.2002.9715305.

[42] Niita K, Sato T, Iwase H, Nose H, Nakashima H, Sihver L. Particle and heavy ion transport code system; PHITS. Radiat Meas. 2006;41:1080–90. doi: 10.1016/j.radmeas.2006.07.013.

[43] Sihver L, Mancusi D, Sato T, Niita K, Iwase H, Iwamoto Y, et al. Recent developments and benchmarking of the PHITS code. Adv Space Res. 2007;40:1320–31. doi: 10.1016/j.asr.2007.02.056.

[44] A.Al-Yousef H, Alotiby M, Kumar A, Alotaibi BM, Alsaif NAM, Sayyed MI, et al. Physical, structural, and gamma ray shielding studies on novel (35 + x) PbO-5TeO_2-20Bi_2O_3-(20-x) MgO-20B_2O_3 glasses. J Aust Ceram Soc. 2021;57:971–81. doi: 10.1007/s41779-021-00600-6.

[45] Alsaif NAM, Al-Ghamdi H, Elsad RA, Abdelghany AM, Shaaban SM, Rammah YS, et al. Fabrication, physical properties and γ-ray shielding factors of high dense B2O3–PbO–Na2O–CdO–ZnO glasses: impact of B2O3/PbO substitution. J Mater Sci: Mater Electron. 2024;35:534. doi: 10.1007/s10854-024-12290-4.

[46] Shaaban KS, Wahab EA, Shaaban ER, Yousef ES, Mahmoud SA. Electronic polarizability, optical basicity and mechanical properties of aluminum lead phosphate glasses. Opt Quantum Electron. 2020;52:125. doi: 10.1007/s11082-020-2191-3.

[47] Sayyed MI, Almuqrin AH, Kumar A, Jecong JFM, Akkurt I. Optical, mechanical properties of TeO_2-CdO-PbO-B_2O_3 glass systems and radiation shielding investigation using EPICS2017 library. Optik. 2021;242:167342. doi: 10.1016/j.ijleo.2021.167342.

[48] Ali AM, Sayyed MI, Rashad M, Kumar A, Kaur R, Aşkın A, et al. Gamma ray shielding behavior of Li_2O-doped PbO–MoO_3–B_2O_3 glass system. Appl Phys A. 2019;125:671. doi: 10.1007/s00339-019-2964-3.

[49] Ilik E, Kavaz E, Kilic G, Issa SAM, Zakaly HMH, Tekin HO. A closer-look on Copper(II) oxide reinforced Calcium-Borate glasses: Fabrication and multiple experimental assessment on optical, structural, physical, and experimental neutron/gamma shielding properties. Ceram Int. 2022;48(5):6780–91. ISSN 0272-8842. doi: 10.1016/j.ceramint.2021.11.229.

[50] Ilik E, Kavaz E, Kilic G, Issa SAM, ALMisned G, Tekin HO. Synthesis and characterization of vanadium(V) oxide reinforced calcium-borate glasses: Experimental assessments on Al_2O_3/BaO_2/ZnO contributions. J Non-Cryst Solids. 2022;580:121397. doi: 10.1016/j.jnoncrysol.2022.121397.

[51] Barebita H, Ferraa S, Moutataouia M, Baach B, Elbadaoui A, Nimour A, et al. Structural investigation of Bi_2O_3-P_2O_5-B_2O_3-V_2O_5 quaternary glass system by Raman, FTIR and thermal analysis. Chem Phys Lett. 2020;760:138031. doi: 10.1016/j.cplett.2020.138031.

[52] Sen Baykal D, Kilic G, İlik E, Kavaz E, ALMisned G, Cakirli RB, et al. Designing a Lead-free and high-density glass for radiation facilities: Synthesis, physical, optical, structural, and experimental gamma-ray transmission properties of newly designed barium-borosilicate glass sample. J Alloy Compd. 2023;965:171392. doi: 10.1016/j.jallcom.2023.171392.

[53] Chandrashekaraiah G, Sivasankara Reddy N, Sujatha B, Viswanatha R, Narayana Reddy C. Role of Er3 + and Bi3 + ions on thermal and optical properties of $Li_2B_4O_7$ glasses: Structural correlation. J Non-Cryst Solids. 2018;498:252–61. doi: 10.1016/j.jnoncrysol.2018.06.034.